Probabilistic Model for Elastic Modulus of Cementitious Materials Reinforced with Carbon Nanotubes

Mahyar Ramezani, Young Hoon Kim*, Zhihui Sun

Department of Civil and Environmental Engineering, University of Louisville, Louisville, KY 40292, USA

Mahyar Ramezani
E-mail: mahyar.ramezani@louisville.edu

Young Hoon Kim
* Corresponding author
Tel: 502-852-4565
E-mail: young.kim@louisville.edu

Zhihui Sun
E-mail: z.sun@louisville.edu

Probabilistic Model for Elastic Modulus of Cementitious Material Reinforced with Carbon Nanotubes

Mahyar Ramezani, Young Hoon Kim, Zhihui Sun

Abstract: Carbon nanotube (CNT) is one of the most promising nanomaterials to increase the elastic modulus of cementitious composites. However, CNT characteristics, dispersion procedure and matrix composition/hydration are critical and correlated with a high degree of uncertainty in achieving a desirable performance. This paper proposes a mechanics-based model to predict the elastic modulus of CNT reinforced cementitious materials based on the Halpin-Tsai equation. The current study employs a probabilistic approach to consider the influences of multiple experimental variables and various sources of uncertainty associated with them. To this end, first, a Bayesian methodology is adopted to perform the model validation, evaluation and selection procedures using extensive literature test data. Then, the optimum ranges of variables are found to maximize the chance of achieving a certain target modulus (herein, 50% more than control) using a reliability analysis. The results indicate that the experimentally observed elastic modulus and the proposed probabilistic model exhibit a similar trend. Therefore, the proposed model can be used to reliably predict the elastic modulus, guiding future researchers to design more efficiently.

Author Keywords: A. Discontinuous reinforcement; B. Elasticity; B. Mechanical properties; C. Analytical Modeling; C. Micro-mechanics

1. Introduction

Elastic modulus correlates stress and strain of a material in the elastic range. It is an important mechanical property because it governs the deformation of a material when it is subjected to external loads. Concerning concrete, the elastic modulus is important for predicting the deflection of structures in service. It also governs the long-term structural behaviors such as creep and relaxation. Therefore, many researchers have tried to improve the elastic modulus using various types and sizes of fibers to produce composite materials in concrete [1, 2]. Fibers, such as steel and carbon, can normally improve the strength of the composite, thus minimizing the risk of cracking and helping to reduce the cross section dimensions. To delay the initiation of cracking, current research tends to use small size fibers, e.g. carbon nanotubes or carbon nanofibers. Recently, the use of carbon nanotubes (CNTs) as the reinforcement in cementitious materials (cement paste, cement mortar and concrete) has attracted considerable attention of researchers [3-6]. Although CNT exhibits the elastic modulus in the order of 1 *TPa* [7, 8] with tensile strength ranges from 11 to 63 *GPa* [9], the elastic modulus of CNT reinfoirced composites is much lower than that of expected with two underlying factors: dispersion quality and bond mechanisms of CTNs within cementitious composites [10, 11]. Some researchers reported that the elastic modulus of CNT reinforced cementitious materials can be significantly increased against the control [3, 12]. While, other researchers reported negligible improvement or even degradation in the elastic modulus [13, 14]. Due to these complexities and non-standardized fabrication procedures, there is yet no model available to reliably predict the elastic modulus of CNT reinforced cementitious materials, hindering the practical application of CNTs in the construction industry.

When CNTs are used to fabricate nanocomposites (e.g., metal, ceramic and polymer), several theoretical models for the elastic modulus exist in the literature. Many researchers attempted to use the conventional theoretical models such as Halpin-Tsai model [15, 16], Mori-Tanaka model [17] and Cox model [18] to recognize the mechanisms of CNTs that affect the elastic modulus of nanocomposites. The conventional models, however, are unable to accurately predict the elastic modulus of nanocomposites in most cases [19, 20], because these models disregard CNT dispersion and bonding characteristics within the hosting matrix. To overcome this, few researchers tried to modify the conventional models by including the CNT aggregation-related constants to fit the model to the experimental test data [21-23]. However, these modified models are empirical (i.e., without a physical meaning) and underestimate the elastic modulus of CNT-reinforced nanocomposites below certain CNT concentrations [21]. Despite some modeling efforts, there are very few published studies that consider the dispersion and bonding mechanisms, simultaneously. Thus, it is essential to consider the influences of CNT dispersion and bonding states in both fabrication and modeling procedures.

In addition, the applicability of the conventional models for CNT reinforced cementitious materials is questionable and has not yet been examined. One of the main reasons is that many researchers reported inconsistent experimental test results concerning the influence of CNTs on the mechanical properties. In fact, the discrepancies are often explained by the degree of CNT dispersion within the matrix and their interfacial bond strength which are influenced by the interactions between multiple experimental variables [24]. Also, the influence of CNTs on the rate of cement hydration has been recently reported [24, 25], yet it was not considered as an important parameter in a mechanics-based model.

The current study aims to propose a mechanics-based model of CNTs in cementitious materials. The proposed model is formulated in a probabilistic manner to improve its robustness against various uncertainty. Toward this end, previously found critical relations to consider the interactions between experimental variables are added to the Halpin-Tsai model to accurately predict the elastic modulus. The accuracy of the proposed probabilistic model is evaluated using extensive experimental test data from the literature. The developed model is then used to identify the best combination of the experimental variables using two approaches: the probability of failure concept and sensitivity and important measures. The details are discussed in the following sections.

2. Modified Halpin-Tsai Model: Previous Study

Amongst various theoretical models, the Halpin-Tsai equation is the most widely used model to predict the elastic modulus of composites because of its simplicity and relative high accuracy [26]. The Halpin-Tsai model has been extensively used to predict the elastic modulus of brittle and ductile materials containing CNTs such as polymers, metals and ceramics [27-31]. It was also used to evaluate the effective elastic moduli of steel-fiber reinforced concrete [32]. The Halpin-Tsai model evaluates the elastic modulus of aligned short fiber reinforced composites in terms of the equivalent fiber and matrix by taking into account the volume fraction of fibers, their geometry (i.e., shape and dimensions) and elastic properties. The general form of the Halpin-Tsai model can be expressed as [15]:

$$E_c = \frac{1 + \xi E_{f'} v_f}{1 - E_{f'} v_f} E_m \qquad (1)$$

where E_c is the elastic modulus of the composite (GPa or *ksi*), E_m is the elastic modulus of the matrix (GPa or *ksi*), ξ is the measure of fiber geometry ($\xi = 2\, {}^{L}/_{d}$ for cylindrical fibers), L is the fiber length (*mm* or *in.*), d is the fiber diameter (*mm* or *in.*), $E_{f'}$ is the equivalent elastic modulus of fiber and v_f is the volume fraction of the fiber which can be calculated using the densities of fiber and matrix. The $E_{f'}$ in the Halpin-Tsai model can be modified to take into account for randomly oriented short discontinuous fibers as follows:

$$E_{f'} = \frac{\chi_o \frac{E_f}{E_m} - 1}{\chi_o \frac{E_f}{E_m} + \xi} \qquad (2)$$

where χ_o is the fiber orientation factor and E_f is the elastic modulus of fiber (GPa or ksi). The χ_o is used to take into account for the possibility of the distributions of discontinuous fibers with different orientations as $\chi_o = \sum_n a_n \cos^4 \Phi_n$ [33], where a_n is the fraction of fibers having orientation angle Φ_n with respect to the reference axis ($\sum_n a_n = 1$). The value of χ_o is one for aligned fibers (the conventional Halpin-Tsai model) and is equal to 3/8 and 1/6 for randomly orientated fibers in two and three dimensions, respectively [34]. Because CNTs are randomly oriented in three dimensions due to their nanoscale sizes, $\chi_o = 1/6$ is considered in this study [21, 22, 35].

As mentioned earlier, the Halpin-Tsai model disregards the influence of CNTs on cement hydration process, their improper dispersion and inadequate adhesion between CNTs and matrix. Therefore, it might lead to inaccurate predictions of the elastic modulus of nanocomposites [19, 20]. To correct this bias and also to understand the mechanisms of CNTs in cementitious materials, the authors' previous study has focused on identifying the most important experimental variables and the interactions between them affecting the mechanical properties including the elastic modulus [24, 25]. The identified important variables include CNT concentration and/or volume fraction (κ and/or v_f), aspect ratio (*AR*), ultrasonication energy (*UE*), ultrasonication amplitude (*UA*), superplasticizer-to-CNTs (*SP/CNTs*) ratio, water-to-cement (*w/c*) ratio, sand-to-cement (*s/c*) ratio and hydration age of cement (*t*). Through extensive experimental and analytical work, three critical relations (dispersion relation [η_D], hydration age relation [η_H], and matrix relation [η_M]) were proposed as follows to include the contributions of multiple variables associated with CNT characteristics, ultrasonication procedure and matrix composition/hydration to the elastic modulus.

1) η_D is to correlate the CNT dispersion as a function of *AR*, CNT volume fraction in aqueous solution (v_{f-w}), *SP/CNTs* ratio and Ultrasonication Energy Indicator (*UEI*).
2) η_M is to include the contributions of *w/c* and *s/c* ratios.
3) η_H is to consider the contributions of κ and *t*.

A brief description of these critical relations is provided in Table 1. More details are provided in the authors' previous study [24]. To validate the applicability of the proposed critical relations to predict the elastic modulus, a simple regression model was developed:

$$E_c = \eta_D{}^{X} \eta_H{}^{Y} \eta_M{}^{Z} E_m \tag{3}$$

where X, Y and Z are the unknown model parameters to fit the data. The unknown model parameters were calibrated using the maximum likelihood parameter estimation function against 84 experimental test data from the literature (see the solid circles in Fig. 1) [24]. The mean values of the calibrated X, Y and Z were reported to be 6.32, 0.43 and 0.22, respectively [24]. A comparison between the predicted (using Eq. (3)) and the experimental elastic modulus is demonstrated in Fig. 1. The 1:1 line (dashed line in Fig. 1) indicates that the predicted elastic modulus is identical to its measured experimental value. Also, the solid lines represent ±20% error. Although Eq. (3) shows an acceptable performance to predict the elastic modulus of the investigated data (see the solid circles in Fig. 1), it is unable to reliably predict the elastic modulus of the new dataset (see the open triangles in Fig. 1). Therefore, the robustness of the regression model is questionable. Besides, the regression model cannot capture the mechanisms of CNTs affecting the elastic modulus. In real applications, the elastic modulus increases as AR and/or v_f increases up to certain thresholds beyond which the elastic modulus degrades due to the dispersion issues. However, when using Eq. (3), the predicted elastic modulus tends to be higher at lower AR and/or v_f. This might be explained by the fact that as AR and/or v_{f-w} decreases, the value of η_D becomes larger (see Table 1). To overcome these limitations, in this study, the proposed analytical relations (η_D, η_H and η_M; see Table 1) are added to the Halpin-Tsai model to predict the elastic modulus:

$$E_c = \eta_D \, \eta_H \, \eta_M \, \frac{1 + \xi E_{f'} v_f}{1 - E_{f'} v_f} E_m \tag{4}$$

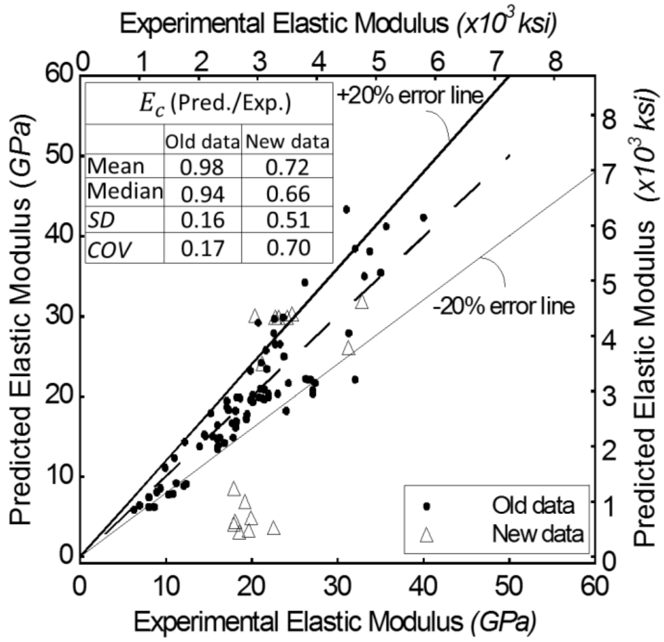

Fig. 1. Experimental versus predicted elastic modulus using Eq. (2)

Table 1. Critical relations affecting the elastic modulus

Critical relation	Equation	Variable (unit)	Mechanism
η_D	$1 - \left[\frac{AR \times v_{f-w}}{UEI \times (SP/_{CNTs})}\right]$	η_D = dispersion relation AR = CNT aspect ratio (unitless) v_{f-w} = CNT volume fraction in aqueous solution (unitless) UEI = ultrasonication energy indicator (index) *SP/CNTs* = superplasticizer-to-CNTs ratio (unitless)	If v_{f-w} or $AR = 0$ (i.e., no CNTs added), $\eta_D = 1$ (perfect dispersion). As v_{f-w} and/or AR increases, η_D gets smaller. As *UEI* and/or *SP/CNTs* ratio increases, η_D gradually reaches one. Beyond certain *UEI* and/or *SP/CNTs* ratio, η_D gets constant.
η_M	$\frac{(1 + {}^{s}/_{c})}{({}^{w}/_{c})}$	η_M = matrix relation ${}^{s}/_{c}$ = sand-to-cemet ratio (unitless) ${}^{w}/_{c}$ = water-to-cement ratio (unitless)	As *w/c* ratio decreases, the value of η_M increases. As *s/c* ratio increases, the value of η_M increases.
η_H	$\left(\frac{t}{4 + 0.85t}\right)^{\kappa}$	η_H = hydration age relation t = age of specimen (days) κ = CNT concentration (*c-wt*%)	If CNT is not added ($\kappa = 0$ *c-wt*%), $\eta_H = 1$. At low CNT concentrations ($\kappa \leq 0.1$ *c-wt*%), the influence of t on η_H is minimal. As κ increases, η_H reaches unity ($\eta_H = 1$) at later ages (i.e., a higher value of t).

Note: $UEI = \left(\frac{UE_T}{UE_m}\right)^{UA}$; UE_T is the total ultrasonication energy (*J/ml*), UE_m is the rate of the ultrasonication process (*J/ml/min*) and *UA* is the ultrasonication amplitude normalized between 0 and 1 [24].

In addition, Eq. (4) is formulated in a probabilistic manner to account for the high degree of uncertainty while incorporating CNTs, statistical uncertainty in estimation of the unknown model parameters, model error associated with inexact form of the model and missing of the possible influential variables [36, 37]. The proposed probabilistic model is then used to identify the most important variables and their optimum ranges using a reliability analysis. This benefits future researchers and designers to identify which variables should be changed to increase the elastic modulus.

3. Formulation of the Proposed Probabilistic Model

This section presents the probabilistic approach based on the available deterministic Halpin-Tsai model (Eq. (1)). Additional correction terms (herein, η_D, η_H and η_M) and model error are introduced to the deterministic expression to account for inherent bias and to capture the remaining variability in residuals, respectively [38]. The probabilistic model relates the quantity of interest (herein, E_c) to a set of measurable variables (defined as $\boldsymbol{x} = (x_1, x_2, x_3, \dots)$) such as *AR*, κ, *UEI*, *SP/CNTs* ratio, *w/c* ratio, *s/c* ratio, *t*, etc. The probabilistic capacity model can be written as follows:

$$C(\boldsymbol{x}, \boldsymbol{\Theta}) = C(\boldsymbol{x}) + \gamma(x, \Theta) + \partial\varepsilon \tag{5}$$

where $C(\boldsymbol{x}, \boldsymbol{\Theta})$ is the capacity model of interest (herein, E_c), $\boldsymbol{x}$ is a set of measurable variables, $\boldsymbol{\Theta} = (\theta, \sigma)$, $\theta = (\theta_1, \theta_2, \theta_3, \dots)$ denotes a set of unknown model parameters used to fit the data, $C(\boldsymbol{x})$ is the selected deterministic model, $\gamma(x, \theta)$ is the correction term (herein, η_D, η_H and η_M), ∂ is a standard deviation of the error term taken from Var $[C(\boldsymbol{x}, \boldsymbol{\Theta})] = \partial^2$, ε is a random variable with zero mean and unit variance and $\partial\varepsilon$ is the error term of the model. There are two assumptions in the formulation of the probabilistic model: 1) ∂ is assumed to be independent of $\boldsymbol{x} = (x_1, x_2, x_3, \dots)$ (i.e., homoscedasticity assumption) and 2) ε has the normal distribution (i.e., normality assumption). The final form of the probabilistic model used to predict the elastic modulus is shown below:

$$E_c = \eta_D(x_D, \theta_D) \times \eta_H(x_H, \theta_H) \times \eta_M(x_M, \theta_M) \times \frac{1 + \xi E_{f'} {v_{f-m}}^{\theta_1}}{1 - E_{f'} {v_{f-m}}^{\theta_1}} E_m + \partial\varepsilon \quad (6)$$

where v_{f-m} is the volume fraction of CNTs within the cement matrix. Note that because v_{f-m} used in cementitious materials is very low (v_{f-m} = 0.000038-0.001277; based on the database), the predicted elastic modulus using the deterministic Halpin-Tsai equation is almost the same as the elastic modulus of the matrix. Therefore, ${v_{f-m}}^{\theta_1}$ is used to fit the data. Also, $\eta_D(x_D, \theta_D) = \left[1 - \left(\frac{AR^{\theta_2} \times {v_{f-w}}^{\theta_4}}{UEI^{\theta_3} \times \left({SP}/{CNTs}\right)^{\theta_5}}\right)\right]$, $\eta_H(x_H, \theta_H) = \left(\frac{t}{4+0.85t}\right)^{\kappa\theta_6}$ and $\eta_M(x_M, \theta_M) = \frac{(1+{S}/{c})^{\theta_7}}{({w}/{c})^{\theta_8}}$ are critical relations after adding the unknown model parameters.

3.1. Bayesian Methodology

A Bayesian methodology is used to correct the impact of each variable in a probabilistic manner. In a Bayesian methodology, the concept of probability is interpreted as the degree of belief of a likelihood of an event by bringing prior knowledge into consideration. The unknown model parameters in Bayesian approach depend on the values of the experimental test data and are estimated using the following updating rule [39]:

$$f(\mathbf{\Theta}) = \lambda L(\mathbf{\Theta}) p(\mathbf{\Theta}) \quad (7)$$

where $\mathbf{\Theta}$ is the vector of unknown parameters, $L(\mathbf{\Theta})$ is the likelihood function that captures the information from data, $p(\mathbf{\Theta})$ is prior distribution that represents the information available before collecting the data, $\lambda = [\int L(\mathbf{\Theta}) p(\mathbf{\Theta})\, f(\mathbf{\Theta})]^{-1}$ is the normalizing factor and $f(\mathbf{\Theta})$ is the posterior distribution that shows the updated state of information about $\mathbf{\Theta}$. Once $f(\mathbf{\Theta})$ is known, the posterior mean vector ($M_{\mathbf{\Theta}}$) and the covariance matrix ($\Sigma_{\mathbf{\Theta\Theta}}$) could be obtained. Because there is no prior information about the unknown model parameters, a non-informative prior distribution $p(\mathbf{\Theta}) \propto \frac{1}{\partial}$ is used [38]. If new data becomes available in the future, Eq. (7) can still be used to update the estimates of the unknown model parameters (i.e., means, variances, and correlation coefficients) by using the current $f(\mathbf{\Theta})$ as a new previous distribution [37].

Table 2. Range of Variables used to Develop Probabilistic Model (Dataset I)

Variables	Minimum	Maximum	Mean	Median	Standard deviation
κ (*c-wt*%)	0.0125	0.5	0.1164	0.1	0.1079
$\boldsymbol{L}$ **(*μm*)**	1.5	55	20.48	20	12.54
$\boldsymbol{d}$ **(*nm*)**	8	32.5	26.86	30	6.72
$\boldsymbol{AR}$ **(unitless)**	157.89	2500	791.02	670.83	536.49
SP/CNTs	1.32	24	5.78	4	4.57
$\boldsymbol{w/c}$	0.3	0.6	0.445	0.485	0.0667
$\boldsymbol{s/c}$	0	3	1.844	2.25	1.18
$\boldsymbol{t}$ **(days)**	3	28	15.44	7	11.24
$\boldsymbol{E_m}$**(*GPa*)**	5.8	27.81	15.24	14.33	5.45
$\boldsymbol{UE_T}$ **(*J/ml*)**	25	2800	1991.85	2800	1119.32
$\boldsymbol{UE_m}$ **(*J/ml/min*)**	3.95	28	9.26	8	5.15
$\boldsymbol{UA}$ **(%)**	30	100	56.44	57	13.78

4. Database for Constructing Probabilistic Model

A total of 105 data is collected from several literature [3, 12, 13, 24, 40-45]. To investigate the robustness of the proposed model, the entire database is not used for the development of the probabilistic model due to two fundamental issues: overfitting and being overly optimistic on model error [46]. There are two common strategies for evaluating the models using the data points that are not being used for model development: creating a hold-out dataset or performing cross validation [47]. In this study, the hold-out method is used to split the database into two sets: the training set (80% of the data; 84 data points) is used to calibrate the unknown model parameters (herein, model development: Dataset I) and the test set (20% of the data; 21 data points) is used to evaluate the accuracy of the estimated unknown model parameters in predicting the elastic modulus of future data(herein, model validation: Dataset II). To split the database, the random subsampling method without replacement is used [47]. Table 2 shows the statistics of different variables used to develop the probabilistic model. Note that the average values of CNT length, diameter and aspect ratio are used in the probabilistic model. For example, if L and d of CNTs are reported to range from 10 to 30 μm and 20 to 40 nm, respectively, L, d and AR of 20 μm, 30 nm and 667 (unitless) are used, respectively.

5. Model Assessment

Table 3 shows the posterior statistics of $\mathbf{\Theta}$ estimated using Dataset I. Also, Fig. 2 shows the performance of the probabilistic model (Eq. (6)) versus the experimental test data. The solid circles are the data used to develop the model (Dataset I) and the open triangles are the data used to validate the model (Dataset II). The robustness of the proposed probabilistic model is validated using Dataset II that was not used for model development, indicating the accuracy of the proposed probabilistic model by showing a desirable performance (i.e., within ± standard deviation of the error term in the proposed model; ∂ = 18%). The proposed probabilistic model after adding the mean values of the unknown model parameters is as follows:

$$E_c = \left[1 - \left(\frac{AR^{0.03} \times {v_{f-w}}^{0.05}}{UEI^{0.03} \times \left({}^{SP}/_{CNTs}\right)^{0.02}}\right)\right] \times \left(\frac{t}{4 + 0.85t}\right)^{2.56\kappa} \times \frac{(1 + {}^{s}/_{c})^{0.46}}{({}^{w}/_{c})^{0.81}} \times \frac{1 + \xi E_{f'} {v_{f-m}}^{0.29}}{1 - E_{f'} {v_{f-m}}^{0.29}} E_m + 0.18\varepsilon \tag{8}$$

Table 3. Posterior Statistics of the Unknown Model Parameters using Dataset I

Unknown parameter	Mean	Standard deviation	Correlation matrix								
			θ_1	θ_2	θ_3	θ_4	θ_5	θ_6	θ_7	θ_8	∂
$\boldsymbol{\theta_1}$	0.2912	0.0230	1	0.6634	0.6766	0.8013	0.0488	-0.3253	-0.5609	-0.3456	0.0676
$\boldsymbol{\theta_2}$	0.0249	0.0089		1	0.6663	0.9061	-0.0037	-0.2431	-0.5304	-0.2254	0.0735
$\boldsymbol{\theta_3}$	0.0257	0.0094			1	0.6288	-0.0826	0.0248	-0.5707	-0.3499	0.1259
$\boldsymbol{\theta_4}$	0.0502	0.0112				1	0.0246	-0.2923	-0.6398	-0.4807	0.0755
$\boldsymbol{\theta_5}$	0.0166	0.0114					1	-0.0709	-0.1251	-0.4773	-0.0311
$\boldsymbol{\theta_6}$	2.5572	0.3296						1	0.2247	0.0285	0.0286
$\boldsymbol{\theta_7}$	0.4624	0.0341				Sym.			1	0.3828	-0.0304
$\boldsymbol{\theta_8}$	0.8091	0.1121								1	-0.0629
$\boldsymbol{\partial}$	0.1803	0.0149									1

To validate the applicability of the proposed critical relations, the corrected relations (i.e., η_D (x_D, θ_D), η_H (x_H, θ_H) and η_M (x_M, θ_M); see Eq. (8)) are further analyzed by comparing the estimated versus the measured values. The estimated value is obtained by plugging in the value of experimental variables in corresponding equations. For example, the estimated value of η_H (x_H, θ_H) is directly calculated using $\eta_H(x_H, \theta_H) = \left(\frac{t}{4+0.85t}\right)^{2.56\kappa}$. Also, the measured value is an indirect back calculation of each critical relation in Eq. (8) using the experimental test results of E_c and E_m. The assumption is that the corrected relations are not correlated.

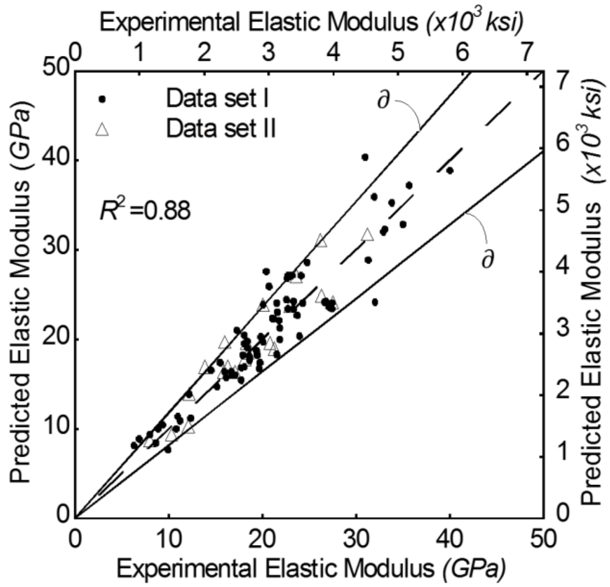

Fig. 2. Predicted value of elastic modulus versus experimental results using Eq. (6) (Dataset I is used for model development and Dataset II is used for model validation)

To visualize the influences of variables on the response (herein, the corrected critical relations), each critical relation is plotted as a function of a main variable and its interaction with another variable in two different ranges: $R1$ and $R2$ (see Table 4) for experimental variable below and above the mean value, respectively. Figs. 3 through 5 demonstrate the influences of the main variables (x-axis) on the corrected critical relations (y-axis). Each plot describes how the response (y-axis) varies as a function of two variables. The solid lines in each plot represent the estimated values of ηs and the dashed lines represent the standard deviation of the model error ($\pm\partial$). To plot the lines, the mean value of other variables is used except for the main variable (x-axis). Also, the open circles represent the measured values of the critical relations. Fig. 3 (a) shows the influence of changes in *AR* and its interaction with another independent variable (v_{f-w}) on η_D (x_D, θ_D). Fig. 3 (b) shows the influence of *UEI* and *SP/CNTs* ratio on η_D (x_D, θ_D). Fig. 4 demonstrates the influence of *t* and its interaction with κ on η_H (x_H, θ_H). And, Fig. 5 shows the contribution of *s/c* ratio and its interaction with *w/c* ratio to η_M (x_M, θ_M).

Table 4. Ranges used for each Critical Relation

Critical relation (*y*-axis)	Main variable (*x*-axis)	Range (based on mean values of data)	
		*R*1	*R*2
η_D^X	*AR*	$v_f \leq 0.0012$	$v_f > 0.0012$
η_D^X	*UEI*	*SP/CNTs* ≤ 5.78	*SP/CNTs* > 5.78
η_H^Y	*t*	κ ≤ 0.1164	κ > 0.1164
η_M^Z	*s/c ratio*	*w/c* ≤ 0.445	*w/c* > 0.445

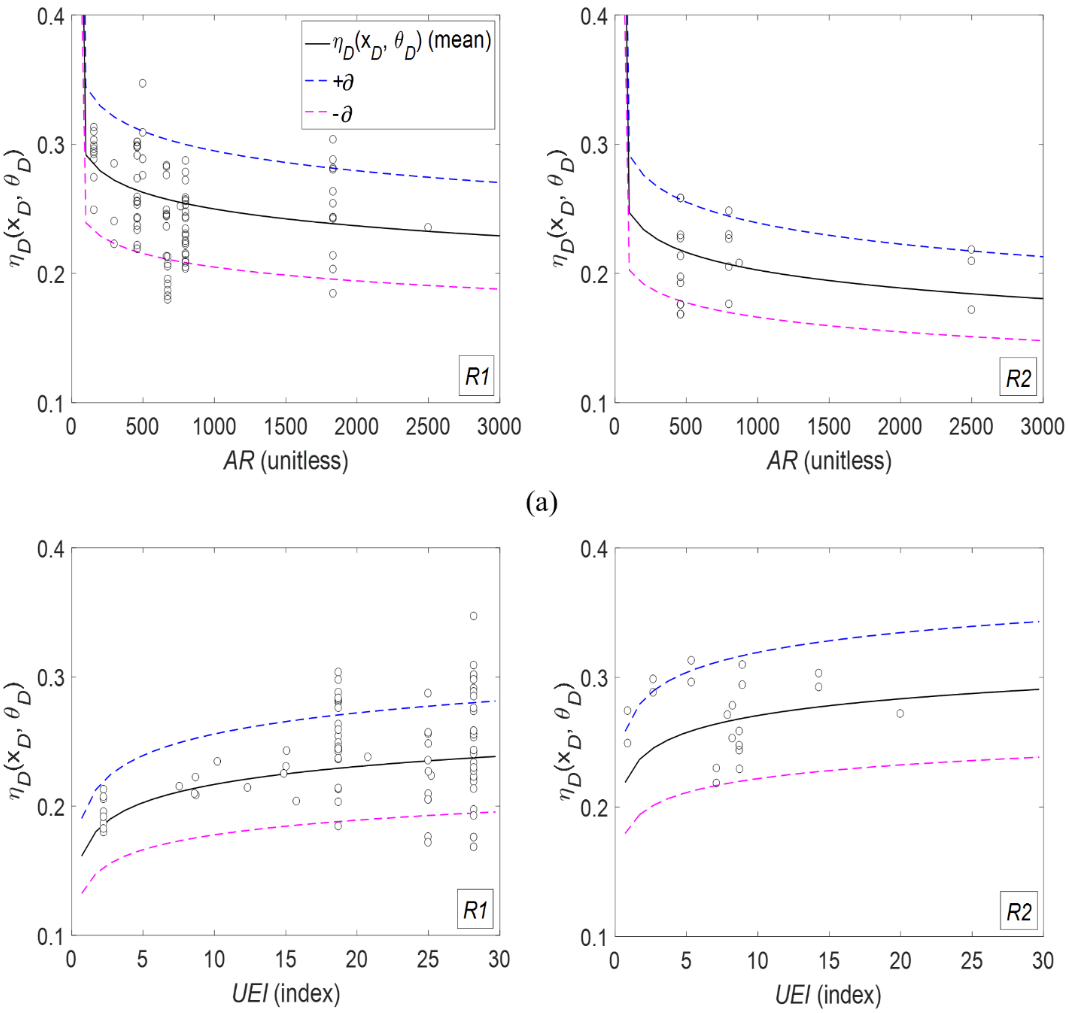

(b)

Fig. 3. Estimated vs. measured η_D (x_D, θ_D) as a function of: (a) *AR* and its interaction with v_{f-w} (b) *UEI* and its interaction with *SP/CNTs* ratio

Figs. 3 through 5 exhibit that most of the measured ηs are within ±∂ and they follow the similar trends as the estimated ηs. For example, Comparing *R*1 and *R*2 in Fig. 4, it is obvious that the influence of *t* on the value of η_H (x_H, θ_H) becomes more pronounced at higher κ (see *R*2 in Fig. 4). Also, Table 5 shows the statistics of the ratio of the measured to the estimated ηs for each data point (the exact values). The mean and median values of the ratio of the measured to the estimated ηs for both ranges are very close to 1.00 with small variations (*COV* ranges between 0.08 and 0.13), indicating that the proposed critical relations can capture the mechanisms of CNTs affecting the elastic modulus of cementitious materials.

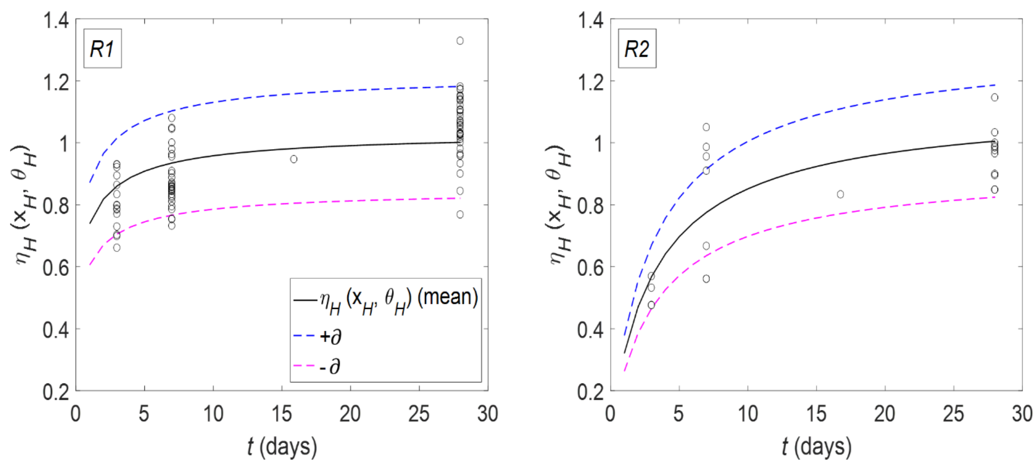

Fig. 4. Estimated vs. measured η_H (x_H, θ_H) as a function of *t* and its interaction with κ

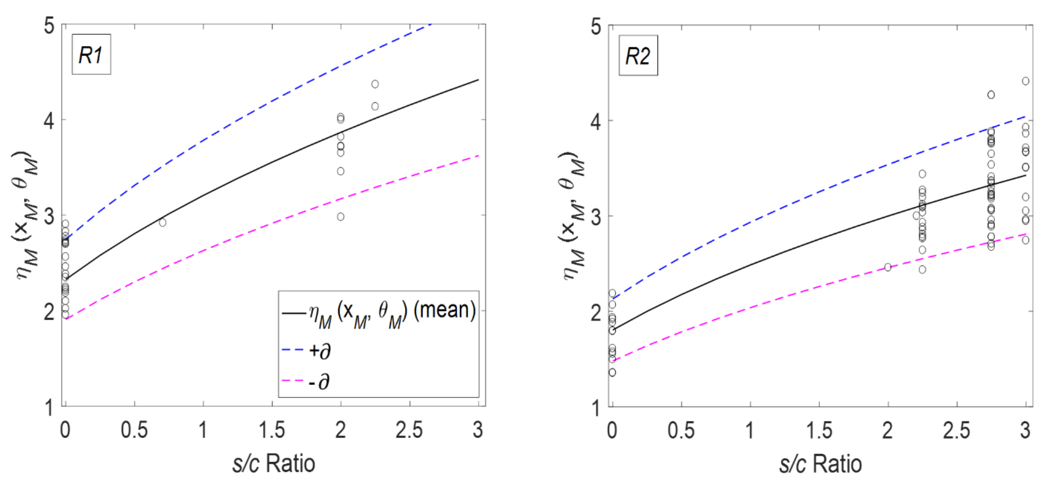

Fig. 5. Estimated vs. measured η_M (x_M, θ_M) as a function of *s/c* ratio and its interaction with *w/c* ratio

Table 5. Statistics of the Ratio of Measured to Estimated Corrected Critical Relations

Critical relation	Main variable	Range	Statistics			
			Mean	Median	Standard deviation	Coefficient of variance
$\eta_D(\boldsymbol{x_D}, \boldsymbol{\theta_D})$	*AR*	R1	1.00	1.01	0.12	0.12
		R2	0.98	0.96	0.13	0.13
$\eta_D(\boldsymbol{x_D}, \boldsymbol{\theta_D})$	*UEI*	R1	0.99	0.98	0.12	0.12
		R2	0.99	1.03	0.12	0.12
$\eta_H(\boldsymbol{x_H}, \boldsymbol{\theta_H})$	*t*	R1	0.99	1.00	0.12	0.12
		R2	1.00	0.98	0.13	0.13
$\eta_M(\boldsymbol{x_M}, \boldsymbol{\theta_M})$	*s/c* ratio	R1	1.02	1.03	0.08	0.08
		R2	0.98	0.97	0.13	0.13

5.1. Model Selection Criteria

For the engineering application purpose, the most complicated model with the highest accuracy may not always be the best model. It is widely accepted that the best model is the one that preserves accuracy of the prediction while using less variables. Therefore, in this study, nine different models containing different subsets of the critical relations are evaluated for model selection (see Table 6). For example, model II only contains the critical relation of η_D with the unity of η_M and η_H (i.e., $\eta_M = \eta_H = 1$). In this regard, a common penalized likelihood information criteria such as Akaike Information Criterion (*AIC*) and Bayesian Information Criterion (*BIC*) can be used to take both model accuracy and parsimony into account. The *AIC* and *BIC* can be determined as follows:

$$AIC = -2\ log\ L(\boldsymbol{\Theta}) + 2N_p \tag{9}$$

$$BIC = -2\ log\ L(\boldsymbol{\Theta}) + N_p log N_s \tag{10}$$

where N_p is number of unknown model parameters included in $\boldsymbol{\Theta}$ and N_s is number of samples. The model with the smallest estimated values of *AIC* and *BIC* is considered as the best model. Table 6 also shows *AIC* and *BIC* estimated values for the competing models. It can be seen that both *AIC* and *BIC* values for model VIII are smaller than those of the other models, indicating that including all critical relations in the probabilistic model leads to a more accurate prediction model.

Also, the R-squared value for model VIII is higher than other candidates, confirming the superior performance of the proposed probabilistic model.

Table 6. Model Selection Criteria using Dataset I

Model		N_p	Information criteria		R-squared
#	Critical relations		AIC	BIC	
I	Deterministic*	1	28.19	28.09	0.63
II	η_D	5	31.78	31.29	0.70
III	η_M	3	19.05	18.76	0.73
IV	η_H	2	23.74	23.55	0.69
V	$\eta_D \times \eta_M$	7	6.83	6.15	0.78
VI	$\eta_D \times \eta_H$	6	31.08	30.50	0.73
VII	$\eta_M \times \eta_H$	4	15.79	15.41	0.76
VIII (Eq. (6))	$\eta_D \times \eta_M \times \eta_H$	8	-2.98	-3.76	0.88
IX (Eq. (1))	Regression^	3	10.31	10.34	0.85

*Halpin-Tsai equation with raising factor θ_1, ^entire data set is used for the regression model

6. Probability of not Meeting Design Specifications

After estimating the unknown model parameters (see Table 3), the proposed probabilistic model (Eq. (6)) is used to optimize each variable through computing the probability of not meeting the specified elastic modulus requirements (probability of failure; P_f). A limit state function $g(\cdot)$ is introduced such that the event $[g(\cdot) \leq 0]$ denotes not meeting the specified capacity requirements [48]. For the determination of the structural reliability, the probability of failure can be derived considering the probability density functions of capacity (C) and demand (D) in the limit state function. If the capacity exceeds the demand (i.e., $C - D > 0$), the structure is safe. Conversely, if the demand exceeds the capacity ($C - D < 0$), the structure fails. The probability of failure could be visualized as the overlapping area of the normally distributed capacity and demand curves (see hatched area in Fig. 6 (a)). In this study, because there is no code or requirement criteria available in the literature, the minimum elastic modulus requirement (demand) of cementitious materials containing CNTs is set to the deterministic value of 50% increase compared with the control (see Fig. 6 (b)). Using the proposed probabilistic model described in Eq. (6), the limit state function can be written as follows:

$$g(\lambda E_m, \boldsymbol{x}, \boldsymbol{\Theta}) = C(\boldsymbol{x}, \boldsymbol{\Theta}) - \lambda E_m \tag{11}$$

where λ is the minimum design requirement (i.e., λ = 1.5). The probability of not meeting the specified elastic modulus requirement can be given by:

$$P(\boldsymbol{\Theta}) = P[g(\lambda E_m, \boldsymbol{x}, \boldsymbol{\Theta}) \leq 0 \mid \boldsymbol{\Theta}] \tag{12}$$

where $P(\cdot \mid \cdot)$ denotes the conditional probability of $g(\lambda E_m, \boldsymbol{x}, \boldsymbol{\Theta}) \leq 0$ for given values of $\boldsymbol{\Theta}$.

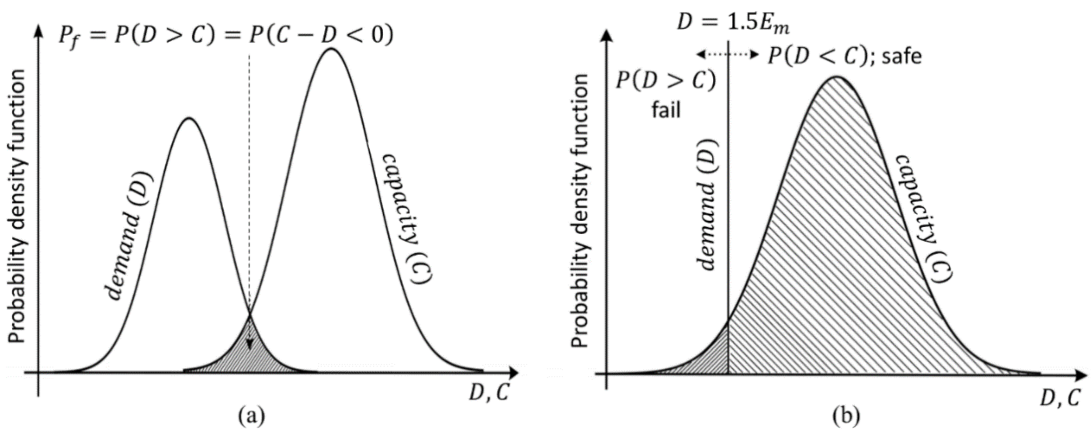

Fig. 6. Reliability analysis using (a) demand and capacity as stochastic parameters; and (b) capacity as a stochastic parameter and demand as a deterministic parameter (modified from [49])

6.1. Relationship between Variables involved in Ultrasonication Procedure

The contour plots of isoprobability lines as functions of UEI versus κ, *AR* and *SP/CNTs* ratio are shown in Fig. 7 (a), (b) and (c), respectively. Note that except for variables in the *x*-axis (e.g., κ in Fig. 7 (a)), the mean value of other random variables is used. The isoprobability lines connect pairs of values of different variables corresponding to the same probability of not meeting the specified elastic modulus requirement ($P[g(1.5E_m, \boldsymbol{x}, \boldsymbol{\Theta}) \leq 0]$). The lower value of isoprobability lines indicates that the chance of obtaining the elastic modulus exceeding 50% larger than the control is higher (lower value of P_f is desirable).

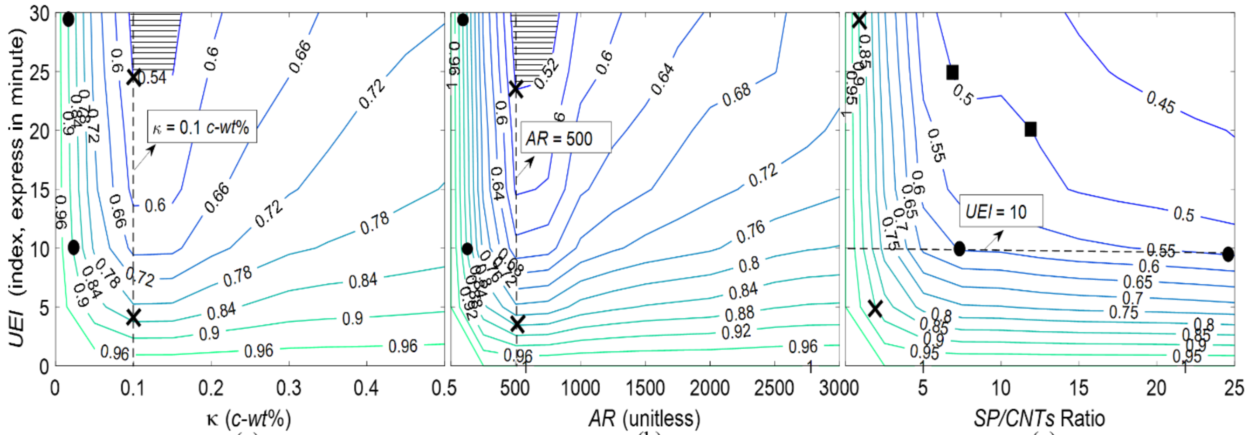

(a) (b) (c)

Fig. 7. Contour plots of the failure probability as functions of (a) *UEI* and κ; (b) *UEI* and *AR*; and (c) *UEI* and *SP/CNTs* ratio

Fig. 7 (a) shows that when κ is below approximately 0.05 *c-wt*%, increasing *UEI* has negligible influence on obtaining higher probability of getting at least 50% increase in the elastic modulus. For example, in case of κ = 0.02 *c-wt*%, the increase in *UEI* from 10 to 30 results in a constant P_f of 0.9 (see the solid circles on the same failure probability line in Fig. 7 (a)). As κ increases, P_f decreases by increasing in *UEI*. For example, in case of κ = 0.1 *c-wt*%, increasing *UEI* from 5 to 25 minimizes P_f (from 0.84 to 0.54; see crosses on the dashed line in Fig. 7 (a)). Generally, P_f is lowest when *UEI* is above 25 and κ is between 0.1 and 0.15 *c-wt*% (see the hatched area in Fig. 7 (a)).

Fig. 7 (b) shows that as *AR* increases, the influence of *UEI* on probability estimates becomes more pronounced. For example, when *AR* = 100, increasing *UEI* from 10 to 30 does not contribute to minimize P_f (i.e., constant P_f of 0.88; see the solid circles on the same failure probability line in Fig. 7 (b)). However, when *AR* = 500, increasing *UEI* from 5 to 24 exhibited the reduction in P_f from 0.8 to 0.52 (see crosses on the dashed line in Fig. 7 (b)). Beyond *AR* = 2500, the increase in *UEI* could reduce P_f, however, the contribution is not significant. Generally, utilizing UEI above 24 with AR between 400 and 800 results in the lowest P_f (see the hatched area in Fig. 7 (b)).

Fig. 7 (c) shows the relationship between UEI and *SP/CNTs* ratio by using contour plot of isoprobability lines. When *SP/CNTs* < 3, increasing UEI has negligible effect on decreasing P_f. This might be attributed to the insufficient *SP* dosage to coat the entire surface of CNTs [50]. For example, when *SP/CNTs* = 2, increasing *UEI* from 10 to 30 results in the same P_f of 0.9 (see the crosses on the same failure probability line in Fig. 7 (c)). In addition, when *UEI* < 10, increasing *SP/CNTs* ratio has minimal influence on the change in P_f. Beyond *UEI* of 10, as *SP/CNTs* ratio increases, lower *UEI* is needed to produce similar P_f. For example, utilizing UEI and *SP/CNTs* ratio of 25 and 7, respectively, results in the same P_f as utilizing UEI and *SP/CNTs* ratio of 20 and 12, respectively, does (see solid squares on the same failure probability line of 0.5 in Fig. 7 (c)). In addition, when *UEI* is fixed, P_f becomes constant beyond certain *SP/CNTs* ratios, and the threshold *SP/CNTs* ratio achieves sooner at lower *UEI*s. For example, when *UEI* = 10, increasing *SP/CNTs* ratio from 7 to 25 does not significantly affect P_f (see solid circles on the dashed line in Fig. 7 (c)). The similar trend was also observed through experimental studies showing that the excessive amount of surfactant-to-CNTs ratio (i.e., beyond their optimum ranges) did not lead to a better dispersion quality [3, 50, 51].

6.2. Relationship between *w/c* and *s/c* Ratios

Fig. 8 shows the contour plot as a function of s/c and w/c ratios based on the fixed values (mean values) of other variables. The probability of failure decreases as s/c ratio increases and/or w/c ratio decreases. For example, in case of *s/c* = 2, the decrease in *w/c* ratio from 0.55 to 0.35 results in the significant decrease in P_f from 0.8 to 0.3 (see solid circles on the dashed line in Fig. 8). In addition, there are several options to achieve the same P_f. For example, utilizing w/c and s/c ratios of 0.35 and 2.25, respectively, results in the same P_f as utilizing w/c and s/c ratios of 0.4 and 3, respectively, does (see crosses on the same failure probability line of 0.25 in Fig. 8).

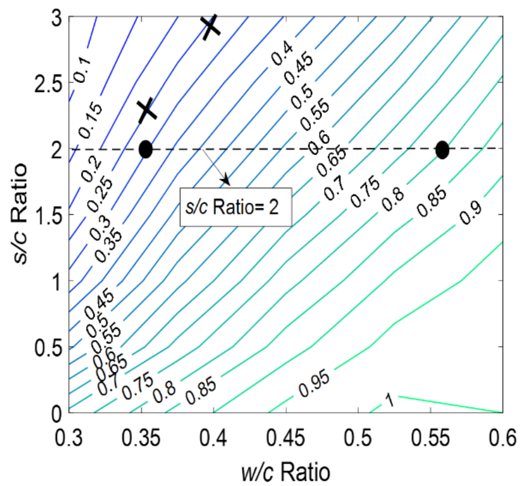

Fig. 8. Contour plot of the failure probability as a function of w/c and s/c ratios

6.3. Relationship between κ and *t*

Fig. 9 shows the relationship between κ and *t* while incorporating mean of other variables. When κ < 0.05 *c-wt*%, *t* has minimal effect on minimizing P_f. However, as κ increases, the effect of *t* on the reduction of P_f is more pronounced. For example, when κ and *t* are 0.1 *c-wt*% and 13 days, respectively, the probability of failure is 0.55. On the other hand, when κ = 0.3 *c-wt*%, *t* = 25 days is required to achieve the same P_f (see crosses on the same failure probability line of 0.55 in Fig. 9). Generally, at low κ, the concentration is the driving force to increase the elastic modulus rather than *t*. As κ increases, the elastic modulus gradually increases against the control (i.e., without CNTs) over time.

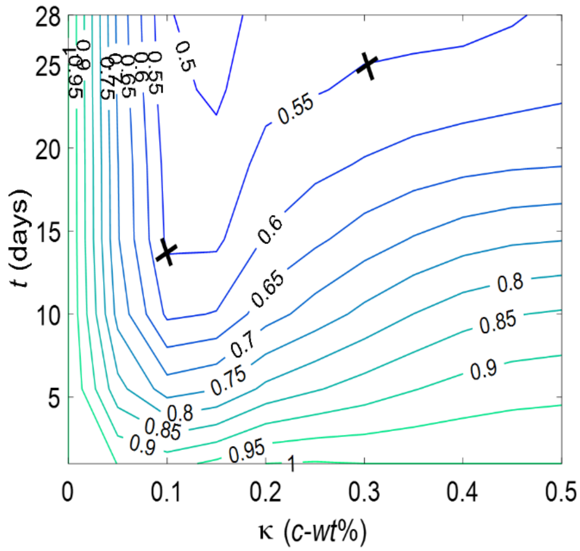

Fig. 9. Contour plot of the failure probability as a function of κ and *t*

6.4. Influence of Optimum Ranges of Variables on Probability Estimates

Fig. 10 shows contour plots of isoprobability lines as a function of κ and *AR* while utilizing mean of other variables (Fig. 10 (a)) or optimum values of each variable (Fig. 10 (b)) obtained from Figs. 7 (c) and 8 (deterministic values: *UEI* = 25, *SP/CNTs* = 7, *w/c* = 0.4, *s/c* = 3). Generally, the value of P_f is very high while incorporating CNTs with high κ and *AR*. Besides, P_f decreases as κ increases up to 0.1 *c-wt*%, beyond which P_f increases, due to the dispersion issues (see dashed lines in Fig. 10).

The lowest P_f is achieved when using CNTs with κ ranges from 0.08 to 0.18 *c-wt*% and *AR* between 400 and 800 (see hatched areas in Fig. 10). In addition, Fig. 10 (b) shows that utilizing optimum ranges of different variables significantly decreases P_f compared to Fig. 10 (a). For example, if using mean value of each variable, the minimum P_f is 0.6 (see hatched area in Fig. 10 (a)). However, when using optimum values of different variables (i.e., deterministic values), the probability of failure decreases to only 0.2 (see hatched area in Fig. 10 (b)). Besides, using either low κ having high *AR* or high κ with low *AR* produces similar P_f. For example, $P_f = 0.2$ can be attained when incorporating either κ = 0.1 *c-wt*% having *AR* = 1000 or κ = 0.18 *c-wt*% having *AR* = 500 (see crosses on the same failure probability line of 0.2 in Fig. 10 (b)). The contour plots also demonstrate the trends observed by other researchers. For example, Konsta-Gdotous et al. [3] and Abu Al-Rub et al. [4] reported that higher concentration of CNTs with smaller aspect ratios produced comparable elastic modulus as lower concentration of higher aspect ratio CNTs did.

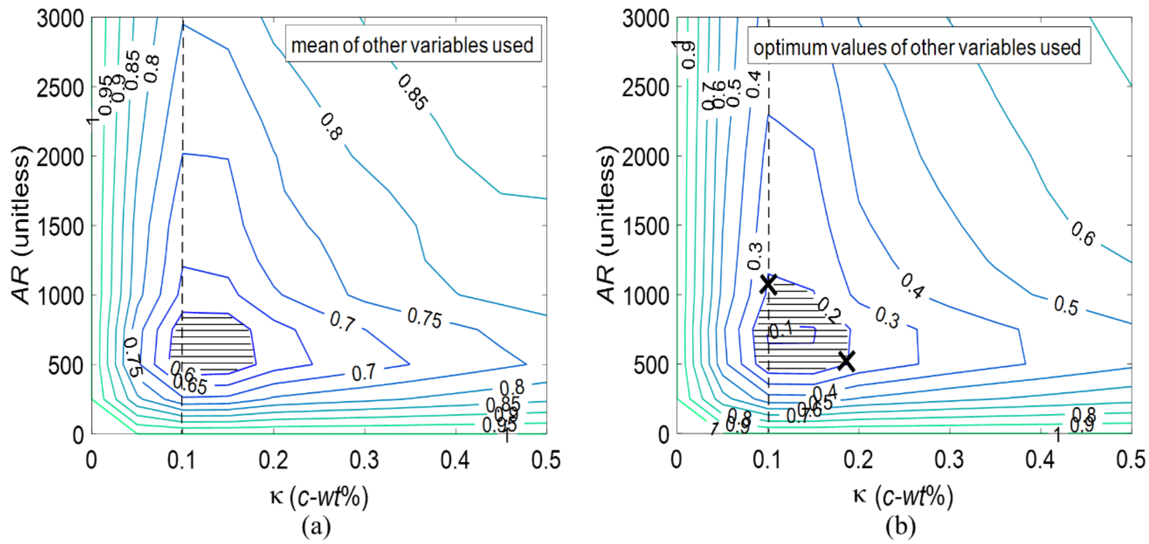

Fig. 10. Contour plots of the failure probability as a function of κ and *AR* when using (a) mean of other variables; and (b) optimum values of other variables

7. Sensitivity and Importance Measures

Sensitivity and importance analyses are performed to determine the effect of different variables on the probability estimates and to gain physical insights. Sensitivity and importance measures could be used to minimize the probability of failure to achieve certain required performance.

7.1. Sensitivity Measure

The sensitivity analysis is performed to investigate what variables are most sensitive to the change of the elastic modulus when design requirement is set to obtaining at least 50% increase compared to the control ($P_f(E_c > 1.5E_m)$) [52]. By computing sensitivity measures, researchers could determine variable(s) to be changed to make stiffer CNT-cement nanocomposites. To compare the sensitivity measures of all the variables, the vector $\boldsymbol{\delta}$ is computed as follows:

$$\boldsymbol{\delta} = \boldsymbol{\sigma_s} \boldsymbol{\nabla}_{\boldsymbol{\Theta}_f} \beta \tag{13}$$

where $\boldsymbol{\sigma_s}$ is the diagonal matrix with diagonal elements given by the standard deviation of each random variable in $\boldsymbol{x}$, $\boldsymbol{\nabla}_{\boldsymbol{\Theta}_f} \beta$ is the gradient vector of β with respect to $\boldsymbol{\Theta}_f$ computed at the mean point and β is the reliability index from first order reliability method (FORM) analysis.

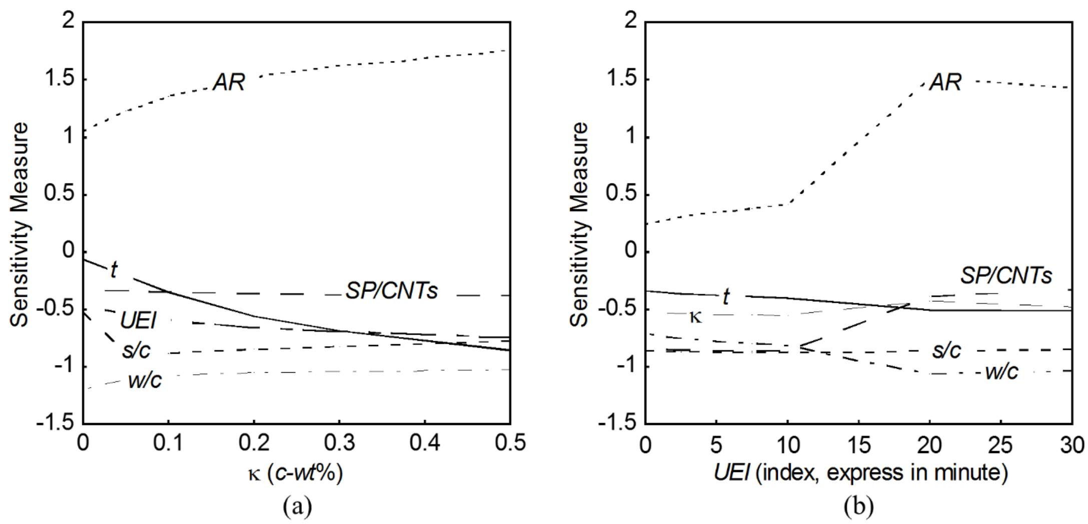

Fig. 11. Sensitivity measure for elastic modulus as functions of (a) κ; and (b) *UEI*

The sensitivity of each variable is measured with respect to two main variables that are believed to significantly affect the elastic modulus: κ and *UEI*. Fig. 11 shows the sensitivity measure of each variable as the change of κ (see Fig. 11 (a)) and *UEI* (see Fig. 11 (b)). Note that the mean of each variable is considered to measure the sensitivity. The higher change in the sensitivity measure (*y*-axis) for each variable with respect to the main variable (*x*-axis) indicates the higher sensitivity of the elastic modulus to the variation in the amount of that variable. For example, Fig. 11 (a) shows that as κ (*x*-axis) increases, *t*, *AR*, and *UEI* have the largest slope amongst other variables, respectively, indicating that they are the most sensitive variables to the change in the elastic modulus. Also, Fig. 11 (b) shows that *AR* and *SP/CNTs* ratio are the most sensitive parameters to the change in the elastic modulus with respect to the change in *UEI*. Conversely, *s/c* ratio and *t* are the least sensitive parameters as a function of *UEI*.

In addition, the negative value of the sensitivity measure for variables (*y*-axis) indicates that P_f decreases as the amount of that variable increases. Conversely, the positive value of the sensitivity measure for each variable indicates that P_f increases as the value of the variable increases. For example, the positive value of the sensitivity measure for *AR* (see Fig. 11) indicates that P_f increases as the value of *AR* increases. On the other hand, Fig. 11 (a) shows that as *t* or *UEI* increases, P_f decreases. As seen in Fig. 11 (b), the negative values of the sensitivity measure for *SP/CNTs* ratio is observed. This shows that P_f decreases as *SP/CNTs* ratio increases. However, *SP/CNTs* ratio gets closer to zero as *UEI* increases. This suggests that lower amount of *SP/CNTs* ratio can be used when higher *UEI* is used. Konsta-Gdoutos et al. [3] also reported that excessive amount of surfactant (i.e., beyond optimum surfactant dosage) degraded the mechanical properties.

7.2. Importance Measure

Although the sensitivity measures provide information on how sensitive the variables are with respect to the changes in the elastic modulus, but they cannot be compared because they have different units [53]. The importance measure can be used to rank the importance of different variables with respect to their effects on the variability of the limit state function.

In the limit state function (Eq. (11)), important variables have larger impacts on the variability of the limit state function and less important variables have smaller impacts. In this research, an importance analysis is conducted to obtain the vector of importance measures ($\boldsymbol{\gamma}$) as follows [54]:

$$\boldsymbol{\gamma}^T = \frac{\boldsymbol{\alpha}^T \boldsymbol{J}_{\boldsymbol{u}^*\boldsymbol{z}^*} \boldsymbol{SD}'}{\|\boldsymbol{\alpha}^T \boldsymbol{J}_{\boldsymbol{u}^*\boldsymbol{z}^*} \boldsymbol{SD}'\|} \tag{14}$$

where $\boldsymbol{\alpha}$ is a row vector of the negative normalized gradient of the limit state function evaluated at the design point in standard normal space, $\boldsymbol{z}$ is vector of random variables ($\boldsymbol{z} = (x_p, \boldsymbol{\Theta})$), $\boldsymbol{J}_{\boldsymbol{u}^*\boldsymbol{z}^*}$ is Jacobian of the probability transformation from the original space (i.e., $\boldsymbol{z}$) to the standard normal space (i.e., $\boldsymbol{u}$) with respect to the coordinates of the most likely failure point (i.e., design point, $\boldsymbol{z}^*$), and $\boldsymbol{SD}'$ is the standard deviation diagonal matrix of equivalent normal variables $\boldsymbol{z}'$ defined by the linearized inverse transformation $\boldsymbol{z}' = \boldsymbol{z}^* + \boldsymbol{J}_{\boldsymbol{z}^*\boldsymbol{u}^*}(\boldsymbol{u} - \boldsymbol{u}^*)$ at the design point. The elements in the matrix $\boldsymbol{SD}'$ are the square root of the corresponding diagonal elements of the covariance matrix $\Sigma' = \boldsymbol{J}_{\boldsymbol{z}^*\boldsymbol{u}^*}\boldsymbol{J}_{\boldsymbol{z}^*\boldsymbol{u}^*}^T$ of the variables in the $\boldsymbol{z}'$.

Fig. 12 shows the importance measures of each variable with respect to κ (Fig. 12 (a)) and *UEI* (Fig. 12 (b)) when using the mean value of other variables. The absolute value of $\boldsymbol{\gamma}$ is a measure of the importance of variables. The higher absolute value of $\boldsymbol{\gamma}$ indicates the higher importance of variables and vice versa. For example, Fig. 12 (a) shows that *s/c* and *w/c* ratios are the most important variables. Also, below κ of 0.1 *c-wt*%, *t* is the least important variable. However, the importance of *t* gradually and consistently increases as κ increases. Besides, as κ increases, the importance of *UEI* increases while the importance of *SP/CNTs* ratio and *w/c* ratio remains constant. As seen in Fig. 12 (b), below *UEI* of around 12, *SP/CNTs* ratio is the most important variable to the change of the elastic modulus. However, the importance of *SP/CNTs* ratio decreases by increasing in *UEI* and it becomes the least important variable above *UEI* of 20 (i.e., the smallest absolute value of importance measure (*y*-axis) amongst other variables). It can also be seen that the importance of κ and *s/c* ratio decreases as *UEI* increases. On the other hand, the importance of *t* and *w/c* ratio remains constant.

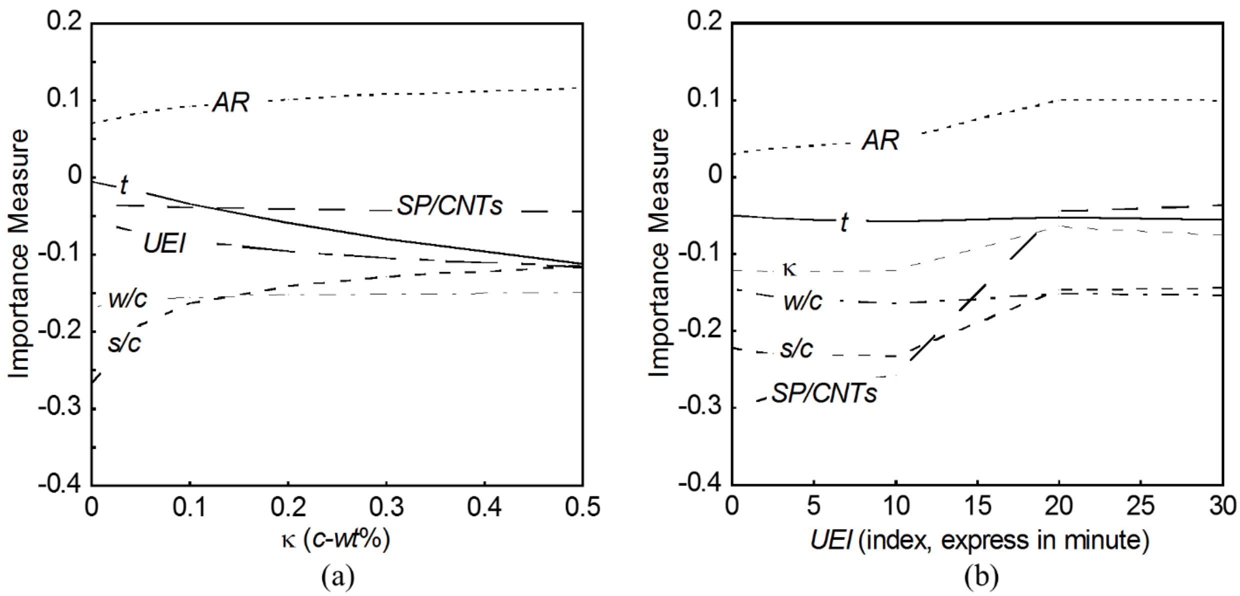

Fig. 12. Importance measure for the elastic modulus as functions of (a) κ; and (b) *UEI*

8. Conclusions

This study proposes a new probabilistic model based on the deterministic Halpin-Tsai equation to predict the elastic modulus of CNT-reinforced cementitious materials (pastes and mortars). The proposed probabilistic model considers the influences of CNT characteristics, dispersion procedure and matrix composition/hydration and is attained using a Bayesian methodology. Then, the conditional probability of failure is used to identify the optimum ranges of experimental variables considered in this study. This facilitates the design of promising nanocomposites through understanding the mechanisms of CNTs in cementitious materials. The following conclusions can be made:

1. The proposed probabilistic model enables to predict the elastic modulus within 18±1% error of the experimental test data (105 data) from the literature including the authors' work.

2. Incorporating CNTs with aspect ratio (*AR*) ranging from 400 to 800 and concentration (κ) between 0.08 and 0.18 *c-wt*% (based on the weight percent of cement powder) results in the highest improvement in the elastic modulus.
3. There are several options to attain the similar elastic modulus with varied combinations of theexperimental variables. Certain combinations of the Ultrasonication Energy Indicator (*UEI*) and superplasticizer-to-CNTs (*SP/CNTs*) ratio or *w/c* and *s/c* ratios might be used to yield similar enhancement in the elastic modulus, when using constant values of other variables.
4. The *AR* and *SP/CNTs* ratio are the most sensitive variables to the change in the elastic modulus with respect to *UEI*. On the other hand, age of specimen and *AR* are the most sensitive variables to change the elastic modulus followed by *UEI* with respect to κ, and their importance increases as κ increases. In addition, the importance of *SP/CNTs* ratio, κ, and *s/c* ratio decreases as *UEI* increases.

References

[1] Yoo, D.-Y., Shin, H.-O., Yang, J.-M., Yoon, Y.-S., Material and bond properties of ultra high performance fiber reinforced concrete with micro steel fibers, Composites Part B: Engineering, 58 (2014) 122-133.

[2] Hannawi, K., Bian, H., Prince-Agbodjan, W., Raghavan, B., Effect of different types of fibers on the microstructure and the mechanical behavior of ultra-high performance fiber-reinforced concretes, Composites Part B: Engineering, 86 (2016) 214-220.

[3] Konsta-Gdoutos, M.S., Metaxa, Z.S., Shah, S.P., Highly dispersed carbon nanotube reinforced cement based materials, Cement and Concrete Research, 40 (2010) 1052-1059.

[4] Al-Rub, R.K.A., Ashour, A., Tyson, B.M., On the aspect ratio effect of multi-walled carbon nanotube reinforcements on the mechanical properties of cementitious nanocomposites, Construction and Building Materials, 35 (2012) 647-655.

[5] Ramezani, M., Kim, Y.H., Hasanzadeh, B., Sun, Z., Influence of carbon nanotubes on scc flowability, 8th INternational RILEM Symposium on Self-Compacting ConcreteWashington DC, USA, 2016, pp. 397-406.

[6] Ramezani, M., Design and predicting performance of carbon nanotube reinforced cementitious materials: Mechanical properties and dipersion characteristics, Electronic Theses and Dissertations (2019) Paper 3255.

[7] Demczyk, B.G., Wang, Y.M., Cumings, J., Hetman, M., Han, W., Zettl, A., *et al.*, Direct mechanical measurement of the tensile strength and elastic modulus of multiwalled carbon nanotubes, Materials Science and Engineering: A, 334 (2002) 173-178.

[8] Wong, E.W., Sheehan, P.E., Lieber, C.M., Nanobeam mechanics: Elasticity, strength, and toughness of nanorods and nanotubes, Science, 277 (1997) 1971-1975.

[9] Yu, M.F., Lourie, O., Dyer, M.J., Moloni, K., Kelly, T.F., Ruoff, R.S., Strength and breaking mechanism of multiwalled carbon nanotubes under tensile load, Science, 287 (2000) 637-640.

[10] Kafi, M.A., Sadeghi-Nik, A., Bahari, A., Sadeghi-Nik, A., Mirshafiei, E., Microstructural characterization and mechanical properties of cementitious mortar containing montmorillonite nanoparticles, Journal of Materials in Civil Engineering, 28 (2016) 04016155.

[11] Sadeghi-Nik, A., Berenjian, J., Bahari, A., Safaei, A.S., Dehestani, M., Modification of microstructure and mechanical properties of cement by nanoparticles through a sustainable development approach, Construction and Building Materials, 155 (2017) 880-891.

[12] Konsta-Gdoutos, M.S., Danoglidis, P.A., Falara, M.G., Nitodas, S.F., Fresh and mechanical properties, and strain sensing of nanomodified cement mortars: The effects of mwcnt aspect ratio, density and functionalization, Cement and Concrete Composites, 82 (2017) 137-151.

[13] Stynoski, P., Mondal, P., Marsh, C., Effects of silica additives on fracture properties of carbon nanotube and carbon fiber reinforced portland cement mortar, Cement and Concrete Composites, 55 (2015) 232-240.

[14] Tyson, B.M., Al-Rub, R.K.A., Yazdanbakhsh, A., Grasley, Z., Carbon nanotubes and carbon nanofibers for enhancing the mechanical properties of nanocomposite cementitious materials, Journal of Materials in Civil Engineering, 23 (2011) 1028-1035.

[15] Halpin, J., Kardos, J., The halpin-tsai equations: A review, Polymer Engineering & Science, 16 (1976) 344-352.

[16] Halpin, J., Tsai, S., Environmental factors in composite materials design. Us air force technical report, AFML TR 67–423, 1967.

[17] Mori, T., Tanaka, K., Average stress in matrix and average elastic energy of materials with misfitting inclusions, Acta metallurgica, 21 (1973) 571-574.

[18] Cox, H., The elasticity and strength of paper and other fibrous materials, British journal of applied physics, 3 (1952) 72.
[19] Zare, Y., Development of halpin-tsai model for polymer nanocomposites assuming interphase properties and nanofiller size, Polymer Testing, 51 (2016) 69-73.
[20] Ayatollahi, M., Shadlou, S., Shokrieh, M., Chitsazzadeh, M., Effect of multi-walled carbon nanotube aspect ratio on mechanical and electrical properties of epoxy-based nanocomposites, Polymer Testing, 30 (2011) 548-556.
[21] Yeh, M.-K., Tai, N.-H., Liu, J.-H., Mechanical behavior of phenolic-based composites reinforced with multi-walled carbon nanotubes, Carbon, 44 (2006) 1-9.
[22] Montazeri, A., Javadpour, J., Khavandi, A., Tcharkhtchi, A., Mohajeri, A., Mechanical properties of multi-walled carbon nanotube/epoxy composites, Materials & Design, 31 (2010) 4202-4208.
[23] Navidfar, A., Trabzon, L., Graphene type dependence of carbon nanotubes/graphene nanoplatelets polyurethane hybrid nanocomposites: Micromechanical modeling and mechanical properties, Composites Part B: Engineering, 176 (2019) 107337.
[24] Ramezani, M., Kim, Y.H., Sun, Z., Modeling the mechanical properties of cementitious materials containing cnts Cement and Concrete Composites, (2019) 103347.
[25] Ramezani, M., Kim, Y.H., Sun, Z., Mechanical properties of carbon nanotube reinforced cementitious materials: Database and statistical analysis, Magazine of Concrete Research, (2019) 1-62.
[26] Mouritz, A.P., Gibson, A.G., Fire properties of polymer composite materials, Springer Science & Business Media2007.
[27] Thostenson, E.T., Chou, T.-W., On the elastic properties of carbon nanotube-based composites: Modelling and characterization, Journal of Physics D: Applied Physics, 36 (2003) 573.
[28] De Villoria, R.G., Miravete, A., Mechanical model to evaluate the effect of the dispersion in nanocomposites, Acta Materialia, 55 (2007) 3025-3031.
[29] Tjong, S.C., Carbon nanotube reinforced composites: Metal and ceramic matrices, John Wiley & Sons2009.
[30] Shokrieh, M.M., Rafiee, R., Investigation of nanotube length effect on the reinforcement efficiency in carbon nanotube based composites, Composite Structures, 92 (2010) 2415-2420.
[31] Chowdhury, S., Haque, B.G., Okabe, T., Gillespie Jr, J., Modeling the effect of statistical variations in length and diameter of randomly oriented cnts on the properties of cnt reinforced nanocomposites, Composites Part B: Engineering, 43 (2012) 1756-1762.
[32] Teng, T.-L., Chu, Y.-A., Chang, F.-A., Chin, H.-S., Calculating the elastic moduli of steel-fiber reinforced concrete using a dedicated empirical formula, Computational materials science, 31 (2004) 337-346.
[33] Krenchel, H., Fibre reinforcement; theoretical and practical investigations of the elasticity and strength of fibre-reinforced materials, (1964).
[34] Rosenthal, J., A model for determining fiber reinforcement efficiencies and fiber orientation in polymer composites, Polymer composites, 13 (1992) 462-466.
[35] Tai, N.-H., Yeh, M.-K., Peng, T.-H., Experimental study and theoretical analysis on the mechanical properties of swnts/phenolic composites, Composites Part B: Engineering, 39 (2008) 926-932.
[36] Tabandeh, A., Gardoni, P., Probabilistic capacity models and fragility estimates for rc columns retrofitted with frp composites, Engineering Structures, 74 (2014) 13-22.
[37] Gardoni, P., Trejo, D., Kim, Y.H., Time-variant strength capacity model for gfrp bars embedded in concrete, Journal of Engineering Mechanics, 139 (2013) 1435-1445.
[38] Gardoni, P., Kiureghian, A.D., Mosalam, K.M., Probabilistic capacity models and fragility estimates for reinforced concrete columns based on experimental observations, Journal of Engineering Mechanics, 128 (2002) 1024-1038.
[39] Box, G.E., Tiao, G.C., Bayesian inference in statistical analysis, John Wiley & Sons2011.

[40] Zou, B., Chen, S.J., Korayem, A.H., Collins, F., Wang, C.M., Duan, W.H., Effect of ultrasonication energy on engineering properties of carbon nanotube reinforced cement pastes, Carbon, 85 (2015) 212-220.
[41] Metaxa, Z.S., Seo, J.W.T., Konsta-Gdoutos, M.S., Hersam, M.C., Shah, S.P., Highly concentrated carbon nanotube admixture for nano-fiber reinforced cementitious materials, Cement and Concrete Composites, 34 (2012) 612-617.
[42] Danoglidis, P.A., Falara, M.G., Katotriotou, M.K., Konsta-Gdoutos, M.S., Gdoutos, E.E., Mwcnt and cnf cementitious nanocomposites for enhanced strength and toughness, Mechanics of Composite and Multi-functional Materials, 7 (2016) 241-246.
[43] Gdoutos, E.E., Konsta-Gdoutos, M.S., Danoglidis, P.A., Portland cement mortar nanocomposites at low carbon nanotube and carbon nanofiber content: A fracture mechanics experimental study, Cement and Concrete Composites, 70 (2016) 110-118.
[44] Gdoutos, E.E., Konsta-Gdoutos, M.S., Danoglidis, P.A., Shah, S.P., Advanced cement based nanocomposites reinforced with mwcnts and cnfs, Frontiers of Structural and Civil Engineering, 10 (2016) 142-149.
[45] Konsta-Gdoutos, M.S., Metaxa, Z.S., Shah, S.P., Multi-scale mechanical and fracture characteristics and early-age strain capacity of high performance carbon nanotube/cement nanocomposites, Cement and Concrete Composites, 32 (2010) 110-115.
[46] Kim, Y.H., Park, Y., Bai, J.-W., Probabilistic shear capacity models for concrete members with internal composite reinforcement, Journal of Composites for Construction, 21 (2016) 04016083.
[47] Weiss, S.M., Kulikowski, C.A., Computer systems that learn: Classification and prediction methods from statistics, neural nets, machine learning, and expert systems, Morgan Kaufmann Publishers Inc.1991.
[48] Ditlevsen, O., Madsen, H.O., Structural reliability methods, Wiley New York1996.
[49] Ranganathan, R., Structural reliability analysis and design, Jaico Publishing House1999.
[50] Sobolkina, A., Mechtcherine, V., Khavrus, V., Maier, D., Mende, M., Ritschel, M., *et al.*, Dispersion of carbon nanotubes and its influence on the mechanical properties of the cement matrix, Cement and Concrete Composites, 34 (2012) 1104-1113.
[51] Yu, J., Grossiord, N., Koning, C.E., Loos, J., Controlling the dispersion of multi-wall carbon nanotubes in aqueous surfactant solution, Carbon, 45 (2007) 618-623.
[52] Hohenbichler, M., Rackwitz, R., Sensitivity and importance measures in structural reliability, Civil Engineering Systems, 3 (1986) 203-209.
[53] Choe, D.-E., Gardoni, P., Rosowsky, D., Closed-form fragility estimates, parameter sensitivity, and bayesian updating for rc columns, Journal of engineering mechanics, 133 (2007) 833-843.
[54] Der Kiureghian, A., Ke, J., Finite-element based reliability analysis of frame structures, Proc. 4th Int. Conference on Structural Safety and Reliability, 1985, pp. 395-404.